CrystEngComm

Cite this: *CrystEngComm*, 2011, **13**, 3569

www.rsc.org/crystengcomm

PAPER

Synthesis and transport properties of Si-doped $In_2O_3(ZnO)_3$ superlattice nanobelts

J. Y. Zhang,[a] Y. Lang,[a] Z. Q. Chu,[b] X. Liu,[a] L. L. Wu[c] and X. T. Zhang*[a]

Received 3rd January 2011, Accepted 24th February 2011
DOI: 10.1039/c1ce00004g

Si-doped $In_2O_3(ZnO)_3$ superlattice nanobelts were synthesized *via* chemical vapor deposition. The transmission electron microscopy result indicates that the nanobelts have a superlattice structure. The introduced Si in $In_2O_3(ZnO)_3$ nanobelts could exist as Si_{Zn} as donor dopants, leading to a low resistivity of 6.25×10^{-3} Ω cm. The transport properties of the nanobelts were measured. A nonlinear *I–V* characteristic is found in a voltage span of 0.4–1.5 V, which is likely attributed to the superlattice structure with statistical potential distribution around the conduction band edge.

Transparent oxide semiconductor (TOS) thin films with high optical transparency and good controllability of carrier generation have been studied intensively for photonic and electronic devices, such as, short-wavelength light emitting diodes and transparent field-effect transistors (TFETs).[1–3] Among the TOSs, a homologous compound $InMO_3(ZnO)_m$ (M = In, Ga, Fe, *etc.*) is a good n-type semiconductor, and has exceptional electron transport properties. The materials have crystal structures belonging to space groups of $R\bar{3}m$ (for m = odd) or $P6_3/mmc$ (m = even), in which alternate stacking of InO_2^- and $MO(ZnO)_m^+$ layers forms periodic layered structures along the [0001] direction.[4] Nomura *et al.* have fabricated $InGaO_3(ZnO)_5$-based TFETs, which exhibit good performances, such as a high on-to-off current ratio of ~10^6 and a high field-effect mobility of ~80 $cm^2\ V^{-1}\ s^{-1}$.[5] However, the TFETs fabricated using conventional TOSs such as SnO_2 and ZnO exhibit poor performance.[6,7] For example, their on-to-off current ratios and field-effect mobilities are of the order of 10^3 and as low as 10 $cm^2\ V^{-1}\ s^{-1}$. Considering the above information, $InMO_3(ZnO)_m$ thin films are a good candidate for TFETs. In addition, with the development of nanoscience and nanotechnology, one-dimensional (1D) $InMO_3(ZnO)_m$ nanostructures have gained utmost concern because of the small size of integrated circuits. Recently a few groups have made important progress in their synthesis by chemical vapor deposition (CVD), such as $In_2O_3(ZnO)_m$ nanowires and nanobelts, $In_2O_3(ZnO)_{10}$ hierarchical superlattice nanostructures, and $ZnO/In_2O_3(ZnO)_m$ heterostructure nanobelts.[8–11] Besides, Wu *et al.* reported the high-yield synthesis of quaternary compound $In_{2-x}Ga_xO_3(ZnO)_3$ nanobelt[12] and Li *et al.* synthesized $InGaO_3(ZnO)_m$ superlattice nanowires.[13] Recently, Huang *et al.* first presented the synthesis of size-dependent $InAlO_3(ZnO)_m$ superlattice nanowires.[14] However, the electron transport properties of 1D $InMO_3(ZnO)_m$ nanostructures have not been reported so far. In this paper, the Si-doped $In_2O_3(ZnO)_3$ nanobelts (SDIZO) were synthesized by CVD. The doped Si behaves as a suitable n-type dopant that gives stable n-type conductivity with high electron concentration. The electron transport properties of the SDIZO nanobelts were investigated.

The SDIZO nanobelts were prepared by CVD. First, the mixture of ZnO, In and Ga used as precursor was placed at one end of an alumina boat and the silicon substrates coated with Au were placed at the other end of the boat which was loaded into a tubular furnace. However, the precursor should be placed at the position of the highest temperature of the furnace. Then the furnace was heated to 1350 °C and kept for 30 min under the flow rate of 100 sccm for N_2 as carrier gas. The pressure was maintained at 300 Pa. At last, the furnace was naturally cooled down to the room temperature. The synthesized products were characterized by scanning electron microscopy (FE-SEM, S-4800, Hitachi), transmission electron microscopy (TEM, Philips Tecnai 20), equipped with an energy dispersive X-ray (EDX) spectrometer. In order to observe the layered structure of superlattice nanobelts, the SDIZO nanobelts were removed from the substrate and embedded with Spurr resin and then they were cut into slices by using a glass knife on a Leica EMUC6 ultra cutter. The electron transport properties were measured by Agilent B1500A.

Fig. 1(a) shows a typical SEM image of the as-synthesized products. A large quantity of nanobelts covers the Si substrate. The length of the nanobelts is in the range of several to tens of micrometres. The width is about 1 μm. The inset in Fig. 1(a) displays an enlarged SEM image.

[a]*Heilongjiang Province Key Lab for Low-Dimensional System and Mesoscopic Physics and School of Physics and Electronic Engineering, Harbin Normal University, Harbin, 150025, People's Republic of China. E-mail: xtzhangzhang@hotmail.com*
[b]*Department of Physics, The Chinese University of Hong Kong, Shatin, Hong Kong, People's Republic of China*
[c]*Center for Engineering Training and Basic Experimentation, Heilongjiang Institute of Science and Technology, Harbin, 150027, People's Republic of China*

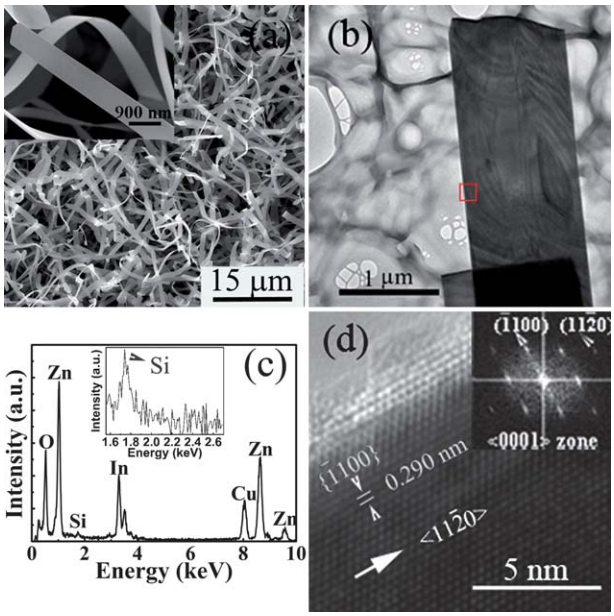

Fig. 1 a) SEM image of the as-grown SDIZO nanobelts; (b) the low-magnification TEM image of a SDIZO nanobelt taken along the ⟨0001⟩ zone axis; (c) the EDX spectrum of a SDIZO nanobelt; (d) the HRTEM of the marked area in Fig. 1(b) and the corresponding fast Fourier transform pattern.

To obtain the detailed information about the morphology and composition of the nanobelts, TEM measurements were performed. Fig. 1(b) shows the low-magnification TEM image of the nanobelt taken along the ⟨0001⟩ zone axis. Each nanobelt is very wide and there is contrast on the surface of the nanobelt due to the internal strain. EDX mirco-analysis on the nanobelt demonstrates that it consists of Si, In, Zn, O, as shown in Fig. 1(c). The Cu signal comes from TEM grid. The atomic ratios of Si, In, Zn, and O are 1.0 : 16.7 : 27.6 : 54.7, which approximately corresponds to the stoichiometric composition of $In_2O_3(ZnO)_3$. Si could be doped into the nanobelts. The internal structure of SDIZO was investigated by HRTEM. Fig. 1(d) shows the HRTEM image of the marked area in Fig. 1(b), taken along the ⟨0001⟩ zone axis. The inset is the corresponding fast Fourier transform pattern. The HRTEM image and the corresponding Fourier transform pattern indicate that: (i) the nanobelts grow along the $[11\bar{2}0]$ direction, with top and bottom surfaces of $\pm\{0001\}$ polar planes and side surfaces of $\{\bar{1}100\}$ planes; (ii) the *d*-spacing between the adjacent $\{\bar{1}100\}$ planes is 0.029 ± 0.002 nm, larger than that of pure ZnO. From the relationship between the *d*-spacing of the adjacent $\{\bar{1}100\}$ planes and the lattice constant, the lattice constant *a* is calculated to be around 0.335 nm, which corresponds well with that of the $In_2O_3(ZnO)_3$.[15]

However, the intrinsic layered structure for $In_2O_3(ZnO)_3$ materials cannot be found in Fig. 1(d). Because the stacking of InO_2^- and $InO(ZnO)_m^+$ layers alternates along the [0001] direction.[9,16] The cross-sectional TEM measurement must be carried out. The sample is prepared by mixing the SDIZO nanobelts with Spurr resin, and crosscutting the mixture into slices of 70 nm thickness. Fig. 2(a) shows a low-magnification TEM image of the slice. The thickness of the nanobelts is about 50 nm, which is consistent with the result of the SEM observation. The selected

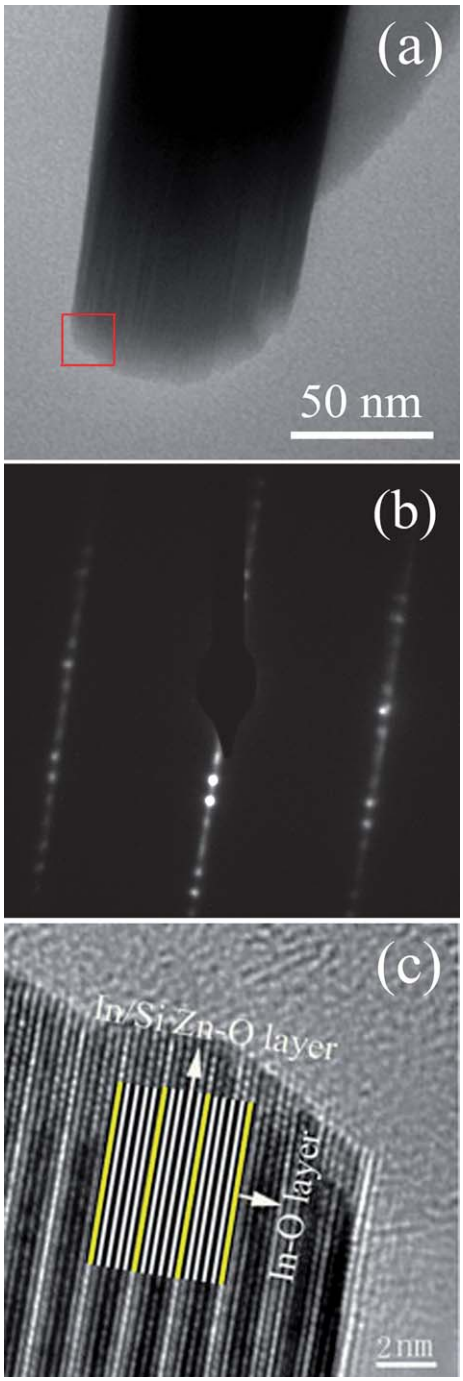

Fig. 2 a) The low-magnification TEM of the slice cut from a SDIZO nanobelt; (b) the selected area electron diffraction pattern of a slice; (c) the HRTEM of the marked area in Fig. 2(a).

area electron diffraction (SAED) pattern taken from a typical slice is shown in Fig. 2(b). A series of satellite diffraction spots are located between two adjacent diffraction spots, indicating the existence of a superlattice structure. Fig. 2(c) shows the HRTEM image of the area marked with the red line in Fig. 2(a). From the HRTEM image, a bright/dark contrast can be clearly observed. The bright contrast corresponds to the In–O layer, the dark to the Si-doped In/Zn–O block. There are four Si-doped In/Zn–O layers between adjacent In–O layers. In^{3+} and Zn^{2+} ions share trigonal bipyramidal and tetrahedral sites in the $InO(ZnO)_m^+$

blocks randomly, which form a random system in the intrinsic crystal structure with the stoichiometric composition. The In–O octahedral layers are inversion boundaries and the polarities at the two sides of the In–O layers are inverted. Thus, the polarities must be inverted again inside the blocks. The Si incorporation in the blocks may facilitate the polarity inversion inside the blocks.[17] Moreover, the distance between the adjacent In–O layers is equal to 1.41 nm. When m is odd, the relevant lattice constant c is 4.23 nm, which corresponds well with that of $In_2O_3(ZnO)_3$.[15] It is also accordant with the formula $d = 6.349 + 2.602m$ Å.[4] It also implies doped Si ions do not cause the obvious variation of the lattice. It is interesting to find at what positions the Si ions appear in the blocks. The Si impurity in SDIZO could in principle occupy the substitutional sites and the interstitial sites forming Si_{Zn}, Si_O, or, Si_i. Among them, Si_{Zn} and Si_O could exist as double donor (Si_{Zn}^{2+}) and acceptor (Si_O^{2-}) in SDIZO, respectively. However, Si_i could exist in acceptor or donor charge states. Lyons *et al.* have calculated that Si_{Zn} is by far the lowest-energy configuration in ZnO. The substitutional configuration Si_{Zn} is lower in energy by at least 10 eV and 3 eV than Si_i and Si_O, respectively.[18] For this reason, Si is likely to substitute the site of Zn in the blocks.

It is known that device performance strongly depends on the quality and transport mechanism of active channel materials. The SDIZO nanobelt device was fabricated, as shown in the bottom-right inset of Fig. 3(a). The device was fabricated following a process below. (i) Some SDIZO nanobelts removed from the Si substrate were dispersed into an ethanol solution. The nanobelts were suspended in the solution using ultrasonic agitation. A droplet of the nanobelt suspension was placed on the thermally oxidized (300 nm) Si substrate. And then a lacy support film was put on the Si substrate; (ii) Ti/Au (20/400 nm) planar electrodes with spacing of 20 μm were deposited on the Si substrate by vacuum evaporation coating, respectively; (iii) in order to make the Ohmic contact between metals and SDIZO nanobelt, the device was annealed at the temperature of 500 °C for 5 min. Then the device was naturally cooled down to the room temperature. The I–V properties were characterized by Agilent B1500A. The special I–V property of the SDIZO nanobelt is observed, as shown in Fig. 3(a), revealing a nonlinear characteristic in a voltage range of −1.5 to 1.5 V, similar to that in the ZnO nanohelix. However, the linear characteristic of the I–V curve (Fig. 3(b)) in a voltage span of −400 to 400 mV indicates that the Ohmic law is obeyed in a low electric field within 20 kV m^{-1}. The resistance is about 25 kΩ. But in a relative high voltage span of 0.4–1.5 V, the nonlinear property appears. The resistance of the belt rapidly reduces to 3 kΩ at 1.5 V. To rule out the effect of the technique on the nonlinear property for the SDIZO device, a pure ZnO nanobelt device was fabricated, as shown in the inset of Fig. 3(c). The ZnO nanobelt device shows an Ohmic transport property (Fig. 3(c)). The fabricating technique and measured condition of the transport property for the ZnO nanobelt device are the same as the SDIZO nanobelt device. The result confirms that the nonlinear property for the SDIZO device is intrinsic and not from the technique. The nonlinear I–V property is likely related with the intrinsic energy band structure of superlattice nanobelts. In^{3+} and Zn^{2+} ions occupy trigonal bipyramidal and tetrahedral sites in the Si-doped $InO(ZnO)_m^+$ blocks randomly, which may lead to the change of electronic

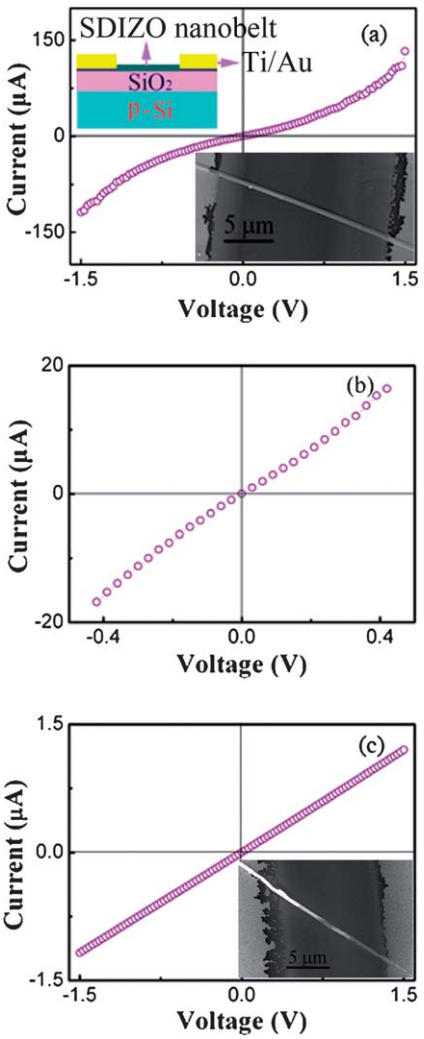

Fig. 3 a) Room-temperature current–voltage characteristic of a SDIZO nanobelt, the top-left schematic is the structure of the fabricated device, the bottom-right picture is an SEM image of the fabricated device; (b) the I–V characteristic of SDIZO nanobelt in the voltage span of −400 to 400 mV; (c) the I–V property of a pure ZnO nanobelt measured under the same experimental conditions and technique. The inset in (c) shows the SEM image of the pure ZnO nanobelt device.

structure around the conduction band edge and formation of the statistical potential distribution.[3,4,19] It is composed of the potential wells and barriers. For the SDIZO device, electron transports in the conductor band have to be tunneling through barriers at a low voltage, and then participate in conduction. So, the I–V curve is linear. However, the thermionic electron emission becomes dominant at a high voltage, which would result in nonlinear I–V characteristic. Wang *et al.* also observed the nonlinear I–V feature in the ZnO nanohelix due to the potential barriers formed at the nanostripe interfaces.[20]

Moreover, the calculated resistivity of the SDIZO nanobelt is as low as 6.25×10^{-3} Ω cm in terms of eqn (1):

$$R = \rho l/s \quad (1)$$

where R is the resistance, l is the spacing between the two electrodes, s is the cross-section, ρ is the resistivity. However, Chen

et al. reported a room-temperature resistivity of 3.12 Ω cm in In–N co-doped ZnO thin films.[21] He *et al.* reported the resistivity of 2.2×10^{-2} Ω cm in the ZnO nanowires.[22] Liao *et al.* reported ZnO nanowires implanted by Ti plasma immersion ion with a varied resistivity from 4.2×10^{2} Ω cm to 3.3×10^{-3} Ω cm.[23] Our results demonstrate that SDIZO superlattice nanobelts have a very low resistivity. The low resistivity could be due to the formation of Si_{Zn} as donor dopants.

In conclusion, SDIZO superlattice nanobelts were synthesized by CVD. The doped Si could behave as donor dopants, resulting in a low resistivity. The electron transport properties of the SDIZO nanobelt devices show a nonlinear characteristic due to the existence of the intrinsic statistical potential distribution. This kind of nanostructure could be used to fabricate nanoscale nonlinear electric devices such varistors, lasers.

Acknowledgements

X.T. Zhang would like to thank supports by the Science Foundation for Distinguished Young Scholars of Heilongjiang Province (JC200805); the Natural Science Foundation of Heilongjiang (A2007-03, A200807 and F200828); the Project of Overseas Talent, Personnel Bureau, Heilongjiang Province.

References

1 H. Ohta, K. Kawamura, M. Orita, M. Hirano, N. Sarukura and H. Hosono, *Appl. Phys. Lett.*, 2000, **77**, 475.
2 A. Kudo, H. Yanagi, K. Ueda, H. Hosono and H. Kawazoe, *Appl. Phys. Lett.*, 1999, **75**, 2851.
3 K. Nomura, T. Kamiya, H. Ohta, K. Ueda, M. Hirano and H. Hosono, *Appl. Phys. Lett.*, 2004, **85**, 1993.
4 N. Kimizuka, M. Isobe and M. Nakamura, *J. Solid State Chem.*, 1995, **116**, 170.
5 K. Nomura, H. Ohta, K. Ueda, T. Kamiya, M. Hirano and H. Hosono, *Science*, 2003, **300**, 1269.
6 M. W. J. Prins, K. O. Grosse-Holz, G. Müller, J. F. M. Cillessen, J. B. Giesbers, R. P. Weening and R. M. Wolf, *Appl. Phys. Lett.*, 1996, **68**, 3650.
7 M. W. J. Prins, S. E. Zinnemers, J. F. M. Cillessen and J. B. Giesbers, *Appl. Phys. Lett.*, 1997, **70**, 458.
8 J. S. Jie, G. Z. Wang, X. H. Hai and J. G. Hou, *J. Phys. Chem. B*, 2004, **108**, 17027.
9 D. P. Li, G. Z. Wang, X. H. Han, J. S. Jie and S. T. Lee, *J. Phys. Chem. C*, 2009, **113**, 5417.
10 B. J. Niu, L. L. Wu and X. T. Zhang, *CrystEngComm*, 2010, **12**, 3305.
11 L. L. Wu, Y. Liang, F. W. Liu, H. Q. Lu, H. Y. Xu, X. T. Zhang and S. K. Hark, *CrystEngComm*, 2010, **12**, 4152.
12 L. L. Wu, F. W. Liu, Z. Q. Chu, Y. Liang, H. Y. Xu, H. Q. Lu, X. T. Zhang, Q. Li and S. K. Hark, *CrystEngComm*, 2010, **12**, 2047.
13 D. P. Li, G. Z. Wang, Q. H. Yang and X. Xie, *J. Phys. Chem. C*, 2009, **113**, 21512.
14 D. L. Huang, L. L. Wu and X. T. Zhang, *J. Phys. Chem. C*, 2010, **114**, 11783.
15 T. Moriga, D. D. Edwards and T. O. Mason, *J. Am. Ceram. Soc.*, 1998, **81**, 1310.
16 B. Alemán, P. Fernández and J. Piqueras, *Appl. Phys. Lett.*, 2009, **95**, 013111.
17 C. W. Na, S. Y. Bae and J. Park, *J. Phys. Chem. B*, 2005, **109**, 12785.
18 J. L. Lyons, A. Janotti and C. G. Van de Walle, *Phys. Rev. B: Condens. Matter Mater. Phys.*, 2009, **80**, 205113.
19 X. T. Zhang, H. Q. Lu, H. Gao, X. J. Wang, H. Y. Xu, Q. Li and S. K. Hark, *Cryst. Growth Des.*, 2009, **9**, 364.
20 P. X. Gao, Y. Ding and Z. L. Wang, *Nano Lett.*, 2009, **9**, 137.
21 L. L. Chen, J. G. Lu, Z. Z. Ye, Y. M. Lin, B. H. Zhao, Y. M. Ye, J. S. Li and L. P. Zhu, *Appl. Phys. Lett.*, 2005, **87**, 252106.
22 J. H. He, P. H. Chang, C. Y. Chen and K. T. Tsai, *Nanotechnology*, 2009, **20**, 135701.
23 L. Liao, Z. Zhang, Y. Yang, B. Yan, H. T. Cao, L. L. Chen, G. P. Li, T. Wu, Z. X. Shen, B. K. Tay, T. Yu and X. W. Sun, *J. Appl. Phys.*, 2008, **104**, 076104.

